Chemical Engineering Research and Design 195 (2023) 355–369

Available online at www.sciencedirect.com

Chemical Engineering Research and Design

journal homepage: www.elsevier.com/locate/cherd

Suspension and flow dynamics of the Allegro™ stirred tank reactor

J.N. Delbridge[a], T.A. Barrett[b], A. Ducci[c], M. Micheletti[a,*]

[a] Department of Biochemical Engineering, University College London, Torrington Place, London WC1E 7JE, United Kingdom

[b] Pall Corporation, Southampton Road, Portsmouth PO6 4BQ, United Kingdom

[c] Department of Mechanical Engineering, University College London, Torrington Place, London WC1E 7JE, United Kingdom

ARTICLE INFO

Article history:
Received 30 March 2023
Received in revised form 17 May 2023
Accepted 23 May 2023
Available online 27 May 2023

Keywords:
Microcarrier suspension
Power input
Cubical vessel
Baffles

ABSTRACT

Microcarrier suspension performance and ensemble-averaged flow fields at the just-suspended condition are studied in a scale-down mimic of the Allegro STR single-use bioreactor range (abbreviated A-STR) and compared to an equivalent standard cylindrical configuration (abbreviated S-STR). Four commercial microcarriers were assessed to determine the required impeller agitation rate and corresponding power input per unit volume to achieve suspension – Cytodex™ 1, Cytodex™ 3, Cytopore™ 1, and Hillex® II microcarriers. The A-STR operating in down-pumping mode (DP) achieved homogenous microcarrier suspension at considerably lower power input when compared to the other baffled configurations. For the A-STR (DP), the power input per unit volume demand was 67.8 % lower than the A-STR in up-pumping mode (UP), 77% lower than the S-STR (DP) and 66.8 % lower than the S-STR (UP). Flow structures investigated at the just-suspended condition, in the transitional regime, were in line with those previously presented in the turbulent regime at considerably higher Reynolds number. This indicates that the normalised flow structures presented in this work are representative of those in the commercial Allegro STR range, despite operating at significantly reduced scale and Reynolds number. Removal of baffles resulted in substantially reduced power input required to achieve homogenous suspension in all configurations – other than the A-STR (DP), which exhibited relatively similar performance to the corresponding baffled configuration. Considering adherent cell sensitivity and mixing implications, and based on the results found in this work, the baffled A-STR (DP) is recommended for achieving microcarrier suspension at the lowest specific power input.

Abbreviations: 2D, two dimensional; 3D, three dimensional; A-STR, Allegro STR bioreactor 1 L prototype; CHO, Chinese hamster ovary; DEAE, diethylaminoethanol; DP, down-pumping; EDR, energy dissipation rate; EE, Elephant Ear impeller; HE-3, Chemineer high efficiency impeller; HEK293, human embryonic kidney 293 cells; hMSC, Human Mesenchymal Stem Cells; LED, light emitting diode; mAb, monoclonal antibody; Mt, megatonne; NS0, murine myeloma cell line; PBT, pitched-blade turbine; PIV, particle image velocimetry; rpm, revolutions per minute; SLA, stereolithography; Sp2/0, murine hybridoma cell line; STR, stirred tank reactor; S-STR, standard stirred tank reactor configuration; SUB, single-use bioreactor; UP, up-pumping

* Corresponding author.
E-mail address: m.micheletti@ucl.ac.uk (M. Micheletti).

https://doi.org/10.1016/j.cherd.2023.05.047

Nomenclature

Roman characters

B_W	Baffle width, [m].
C	Impeller clearance from tank bottom to mid-impeller, [m].
D	Impeller diameter, [m].
F	Force exerted on gauge due to impeller motion, [N].
H	Bioreactor height, [m].
H	Homogeneity index, [%].
H_L	Liquid height, [m[.
I_o	Image intensity with settled microcarriers, [-].
I_{max}	Image intensity for homogenous suspension, [-].
l	Lever arm, [m].
N	Impeller rotational speed, [s^{-1}].
N_H	Minimum speed to homogeneity, [s^{-1}].
N_{JS}	Just-suspended speed, [rpm].
n	Number of experimental repeats, [-].
N_P	Impeller power number, [-].
P	Power input, [W].
T	Vessel internal diameter, [m].
t_H	Time to homogenous suspension, [s].
T_q	Impeller torque, [N m].
r	Radial distance, [m].
Re	Reynolds number, [-].
$\bar{U}_{rz}$	Ensemble-averaged magnitude of radial and axial velocity components, [m s^{-1}].
V_{tip}	Impeller tip velocity, [ms^{-1}].
V	Liquid volume, [m^3].
W	Impeller height, [m].
z	Axial distance, [m].

Greek characters

θ	Tangential direction angle, [deg].
$\epsilon_{T\,max}$	Maximum energy dissipation rate, [W kg^{-1}].
$\bar{\epsilon}_T$	Ensemble-averaged energy dissipation rate, [W kg^{-1}].
λ	Wavelength, [nm].
μ	Dynamic viscosity, [kg m^{-1} s^{-1}].
ν	Kinematic viscosity, [m^2 s^{-1}].
ρ_L	Fluid density, [kg m^{-3}].

1. Introduction

The use of stirred tank reactors for solid-liquid suspensions is common in several biochemical engineering applications, and more so in recent years with the drive towards biopharmaceuticals and adherent stem cell-based products. Most large-scale therapeutic protein production involves suspended mammalian cell culture – for instance the use of CHO, NSO, HEK293, or Sp2/0 cells for production of therapeutic proteins (Allan et al., 2019). However, in some cases cells require a scaffold for growth and are proliferated on suspended microcarriers. Common applications include cultivated meat production (Hanga, 2020) and human mesenchymal stem cell (hMSC) expansion for regenerative medicine products (Nienow, 2014; Jossen, 2018). As an example, hMSCs are being investigated in over 300 clinical trials with potential benefits for diabetes, organ transplantation, Crohn's disease, brain and spinal cord injuries to name a few (Schirmaier, 2014; Silva Couto, 2019). A single patient dose can usually be produced in planar culture or a bench-scale bioreactor, but to meet the current demand for multiple patients, robust cell culture processes in bioreactors at the 10–200 L scale would be highly beneficial (Lawson, 2017). One of the first studies regarding production of functional hMSCs in a stirred tank reactor at the litre scale was reported by Rafiq et al. (Rafiq, 2013). More recent literature has reported production volumes of anchorage-dependent MSCs in 35–50 L single use STRs (Schirmaier, 2014; Lawson, 2017; Jossen, 2018). This contrasts the scale of therapeutic protein production by suspended animal cell culture at volumes of up to 20,000 L (Allan et al., 2019). Cultured meat production – a very different application of suspended microcarrier culture – faces its own challenges. The predicted meat demand increase of 48 Mt by 2025 makes cultured meat an appealing alternative to farmed animal products given the reduced land occupation, water usage, greenhouse gas emissions, and not to mention the animal welfare prospects and reduction in animal borne diseases (Hanga, 2020; Garrison et al., 2022). However, despite major cost reductions since the first cell-cultured hamburger valued at $325 000 ($2.3 million/kg) (Garrison et al., 2022), further decreases in production costs are essential to make cultured meat an economically viable alternative to conventional meat. Whether to achieve clinically-relevant numbers of anchorage-dependent cells or to combat the ever-growing food crisis, process development for microcarrier suspension at large-scale is key to meet demands and reduce process costs (Nienow et al., 2016). Characterisation of microcarrier suspension processes in stirred tank reactors can facilitate process scale-up, benefit from economies of scale, achieve greater consistency in product quality due to improved process monitoring and control, and assist in meeting regulatory demands (Lawson, 2017; Silva Couto, 2020).

The sensitivity of mammalian cell types to hydrodynamic forces has been somewhat overestimated in suspended cell culture applications, where studies have shown cells to be considerably more robust than previously suspected (Ma et al., 2002; Mollet, 2007; Godoy-Silva, 2009; Godoy-Silva et al., 2009; Nienow, 2013; Neunstoecklin, 2015; Neunstoecklin, 2016; Nienow, 2021). In microcarrier suspensions the implications of hydrodynamic forces are more significant, causing detachment of anchorage-dependent cells from their microcarrier scaffolds and consequent cell death (Allan et al., 2019). A minimum ensemble-averaged specific energy dissipation rate ($\bar{\epsilon}_T$) is thus targeted for microcarrier suspension applications, however, mass transfer of nutrients and unwanted metabolites should not be compromised by low power input (Nienow et al., 2016). STRs are thus typically operated in the just-suspended state for microcarrier suspensions, where the impeller is operated at the minimum speed (N_{JS}) to fully suspend the microcarrier population and the corresponding mean (ensemble-averaged) specific energy dissipation rate set as the minimum (Nienow et al., 2016). Mean specific EDRs, $\bar{\epsilon}_T$, are generally derived from impeller power input, but in reality, the local EDR in stirred tanks can reach significantly higher magnitudes in the impeller region.

$$\epsilon_{T\,max} = \Phi\bar{\epsilon}_T \quad (1)$$

Values of Φ reported vary for impeller type and D/T ratio, and range from 10 to over 100, with values generally being smaller for larger D/T ratios (Nienow, 2014). Typically a value of Φ = 30 is used for studies regarding biological entities, but an accurate value is challenging to determine experimentally

(Nienow et al., 2014, 2016). Ducci and Yianneskis (2005) determined that Φ could reach up to 36 in the impeller region of a Rushton turbine. Furthermore, studies on the periodic variation of EDR in stirred tanks have found that the instantaneous value for $\epsilon_{T\,max}$ can reach up to 80 times $\bar{\epsilon}_T$ (Micheletti, 2004; Huchet et al., 2009). Hydrodynamic forces due to agitation can actually benefit microcarrier suspension, from which the harvest of the final cell product has proved difficult (Nienow et al., 2014; Koh et al., 2020). Enzymatic detachment of cells from microcarriers has been improved by intense agitation at 5 times N_{JS}, where the corresponding Kolmogorov microscale was small enough to remove cells from 200 µm microcarriers, but larger than the freely suspended cells thus avoiding cell damage (Nienow et al., 2014, 2016). The interplay between mixing and suspension performance and the consequent flow and shear conditions have been explored in a DASGIP reactor for both continuous and intermittent agitation (Samaras et al., 2019, 2020). Wyrobnik et al. (2022) assessed the same conditions in a Sartorius Univessel comparing a marine impeller, 3-blade segment (Elephant Ear) impeller, as well as a novel impeller design. Collignon et al. (2016) used Large Eddy Simulation (LES) to evaluate the energy dissipation rates of a Rushton turbine, EE impeller, and marine impeller at N_{JS}.

This work focuses on characterisation of suspension dynamics in the geometry of Pall Corporation's single-use Allegro™ STR bioreactor range. The Elephant Ear (EE) impeller incorporated into the Allegro STR design is particularly well suited to microcarrier suspension applications. Collignon et al. (2010) compared the mean flow fields of several axial impellers at the just-suspended speed and determined that the EE impeller resulted in the lowest shear rate. In this work, suspension dynamics of the EE impeller in the Allegro STR is compared to that of a standard stirred tank configuration, to determine the influence of the Allegro STR's unique geometry. At low D/T ratios (D/T < 0.5), Mitchell et al. (2008) determined N_{JS} for a pitched-blade turbine (PBT) and hydrofoil in a flat bottom square tank to be higher than that in a cylindrical tank, due to the increased distance to the corners of the square tank and the tendency of solids to pile-up in this region. However, at higher D/T ratios the square tank exhibited improved suspension efficiency due to reduced likelihood of solid piles forming below the impeller when compared to the cylindrical geometry (Mitchell et al., 2008). Giacomelli et al. (2023) found the point of last suspension in a square vessel stirred by a PBT or hydrofoil impeller to be at the corners of the vessel base, due to dampened flow and turbulence in this region. In contrast, Collignon et al. (2015) investigated the flow pattern in a parallelepiped disposable bioreactor geometry, and found velocities up to 5 % of the impeller tip speed in the tank corners, indicating no stagnant region was present. Suspension studies on the cuboidal Ambr® 15 found that pre-treatment was necessary to prevent microcarriers settling in the tank corners, however, cells proliferated and maintained their quality attributes despite operating at higher $\bar{\epsilon}_T$ than typically considered acceptable for microcarriers (Nienow et al., 2016). The Allegro STR 50 was used to culture hMSCs on Solohill microcarriers at 30 L scale (Bayne et al., 2019). The single-use biocontainer of the Allegro STR, while cubical, forms rounded edges when inflated in the surrounding support structure with the aim of preventing mixing dead zones (Nienow et al., 2016). The present work was motivated by Professor Alvin Nienow's contribution to the design of the Allegro STR bioreactor range, designed with his valuable input and knowledge of stirred tanks and the field of mixing. The study aims to shed light on the impact of vessel geometry, impeller pumping direction, and the presence of baffles on the quality of suspension.

Previous work characterised power, mixing and flow at typical power input in a scale-down prototype of the Allegro STR and a standard cylindrical STR of equivalent proportions for comparison (Delbridge et al., 2023). Agreement of turbulent power number and mixing number data with that of the commercial Allegro STR 50 – 2000 L range indicated good scalability (Delbridge et al., 2023). In the current work, the same transparent scale-down 1 L prototype of the Allegro STR was used for suspension characterisation studies, to determine the influence of its cubical geometry and baffle design. Microcarrier suspension and flow structure at the just-suspended speed in the scale-down 1 L Allegro STR is compared to that in an equivalent cylindrical standard bioreactor geometry, stirred by the same Elephant Ear impeller design.

2. Materials and methods

2.1. Bioreactor configuration

Measurements were obtained in a scale-down prototype of the Allegro STR 50–2000 L bioreactor range, previously described in Delbridge et al., (Delbridge et al., 2023). The 1 L prototype (abbreviated A-STR) was scaled from dimensions of the Allegro STR 50 biocontainer (Pall Corporation, Portsmouth, United Kingdom) and fabricated from transparent acrylic. A 'standard' dished bottom cylindrical vessel (abbreviated S-STR) stirred by the same 3-bladed 45° pitched-blade Elephant Ear impeller design was characterised for comparison. Characteristic ratios, D/T = 0.5, C/T = 0.25, and W/D = 0.5, were maintained across the two vessels. D, T, C and W represent the impeller and tank diameters, mid-impeller off-bottom clearance, and blade height respectively (Fig. 1). The S-STR was slightly larger in size compared to the A-STR (T = 0.11 m vs T = 0.10 m). All measurements were taken at a non-dimensional liquid height of $H_L/T = 1.1$, corresponding to a working volume of 1 L in the baffled A-STR and 1.1 L in the S-STR. Four standard 'flat-pate' baffles of width $B_W/T = 0.1$ were incorporated in the S-STR, while the A-STR was operated with three asymmetrically placed wedge-shaped baffles as found in the commercial Allegro STR range. Both the S-STR and A-STR were also operated without baffles to determine the impact on suspension dynamics and flow pattern. The unbaffled and baffled configurations were assessed in both up-pumping (UP) and down-pumping (DP) modes, where UP mode corresponds to anti-clockwise impeller rotation and vice versa.

2.2. Impeller power input characterisation

Given the common use of power input per unit volume (P/V) to scale mammalian cell culture, the power input of the A-STR and S-STR was determined for the agitation range across which suspension was assessed. This was carried out to provide an unbiased comparison of suspension efficiency between the two vessel configurations, given that their impeller power input would vary considerably at the same agitation rate. A frictionless air-bearing system supplied with pressurised air at 0.25 bar was used to determine impeller

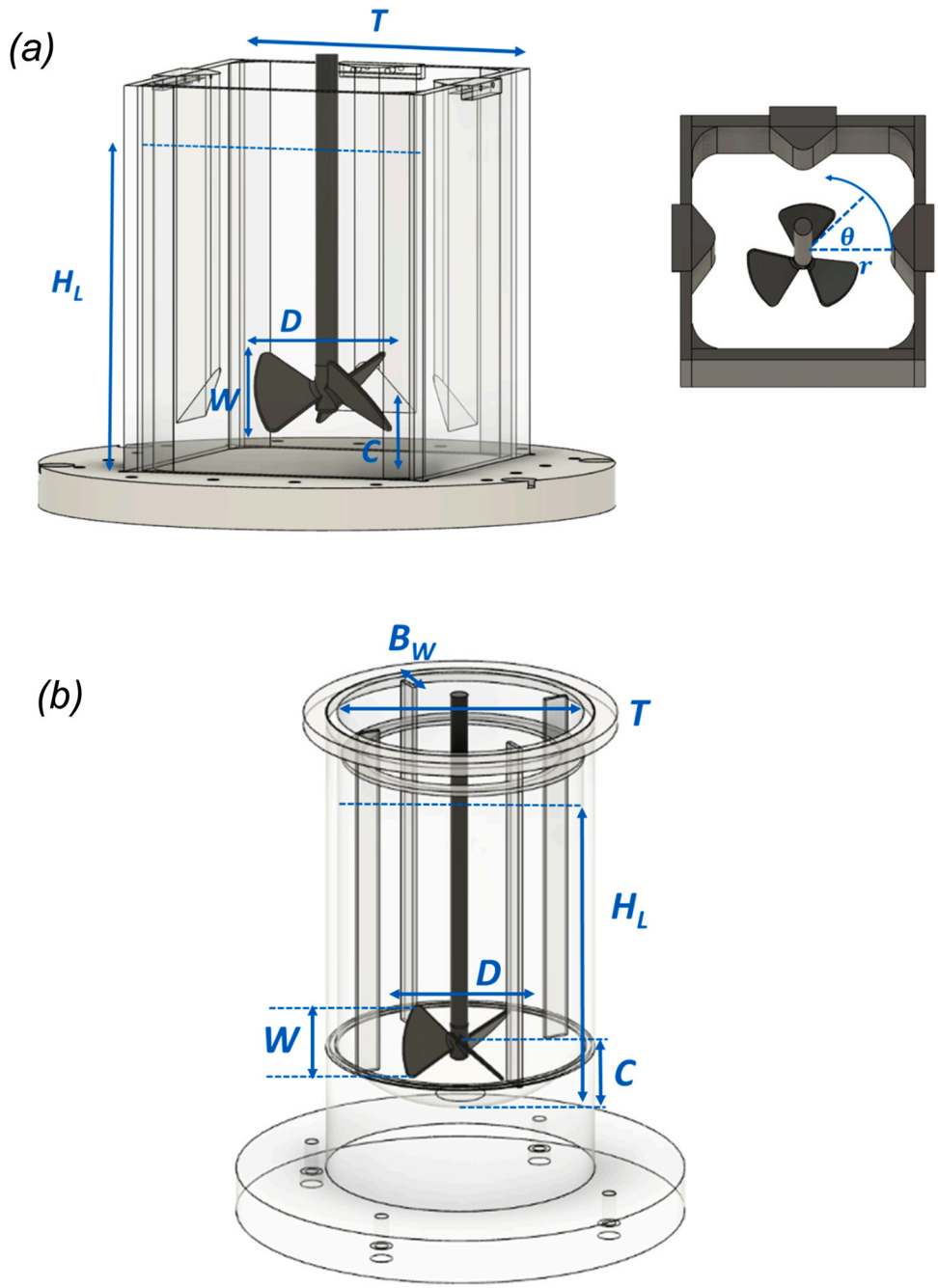

Fig. 1 – (a) Scale-down 1 L prototype (abbreviated A-STR) of the Allegro STR geometry, with top view shown to distinguish between planes based on azimuthal coordinate, θ, increasing in the anti-clockwise direction; (b) Hemispherical bottom cylindrical STR (S-STR) with standard baffling and equivalent geometric proportions to the A-STR.

power input for each configuration at Reynolds numbers ranging from Re = 1–2 × 10^4. To cover the broad range of Re (Eq. 2), mixtures of glycerol (Fisher Scientific, UK) and ultra-pure Milli-Q® water were used to modify the rheological properties of the working fluid.

$$\mathrm{Re} = \frac{ND^2\rho_L}{\mu} \tag{2}$$

Where N is the impeller agitation rate, ρ_L is the working fluid density, and μ is the working fluid dynamic viscosity. A digital force gauge (Omega Engineering, UK) was used to obtain force readings at each condition. The power input (Eq. 3) and impeller power number (Eq. 4) were determined at each Reynolds number using average force readings (n = 3).

$$P = 2\pi NlF = 2\pi NT_q \tag{3}$$

$$N_P = \frac{P}{\rho_L N^3 D^5} \tag{4}$$

Where P is the power input, N the impeller agitation rate, l is the force lever arm, and F the measured force. A detailed description of the apparatus and system set-up is given in a previous work regarding the characterisation of the A-STR and S-STR (Delbridge et al., 2023). Piecewise linear interpolation was applied to the power curve data to obtain the power number at specific Re.

2.3. *Microcarrier suspension characterisation*

Microcarrier suspension characterisation was carried out for each of the STR configurations shown in Fig. 1. The S-STR was placed in a water-filled glass trough to minimise optical

Table 1 – Characteristics of commercial microcarriers assessed in suspension study.

	Cytodex 1	Cytodex 3	Cytopore 1	SoloHill Hillex
Specific gravity (g/cm^3)	1.03	1.04	1.03	1.08 – 1.15
D_{50} (wet) (μm)	190	175	230	180
Nominal surface area per gram (cm^2/g)	4400	2700	11,000	500
Dry weight used (g/L)	0.91	1.48	0.36	8
Manufacturer	Cytiva	Cytiva	Cytiva	Sartorius

distortion due to the curvature of the vessel's external surface. This was not required for the cubical A-STR. An illuminated LED panel (580 mcd) was placed behind the vessel to obtain a background of homogenous intensity. Four commercially available microcarriers were used for suspension dynamics characterisation: Cytodex™ 1, Cytodex™ 3, Cytopore™ 1, and SoloHill® Hillex® II microcarriers (Table 1).

Microcarriers were stained with 0.4 % Trypan Blue (Sigma-Aldrich, USA) for improved visualisation (Olmos, 2015; Samaras et al., 2020). To obtain a total microcarrier surface area of approximately 4 cm^2/mL, microcarrier solutions were prepared in ultrapure Milli-Q water at varied concentration depending on their nominal surface area per gram. Studies regarding culture of anchorage-dependent cell lines recommend a microcarrier concentration of 4–5 cm^2/mL (Nienow, 2014; PALL, 2015). To assess microcarrier suspension with increasing impeller power input, an agitation range of 5–200 RPM was investigated in both the A-STR and S-STR. At each agitation rate, images were acquired for 5 min at a frequency of 2 Hz using an iCube camera (NET, Germany) focused on the front face of the vessel. Microcarriers were left to fully settle between adjustments of the agitation rate. Images acquired at each agitation rate were processed using a purposely written MATLAB code. A homogenous distribution of microcarriers across the vessel volume is considered to be achieved when the suspension homogeneity index, H (N), defined in Eq. (5) is equal to one (Samaras et al., 2020):

$$H(N) = \frac{(I_0 - I_N)}{(I_0 - I_{max})} \quad (5)$$

where I_0 is the brightness across the measured plane of view before agitation takes place, I_N is the cumulative brightness at each speed (N), and I_{max} corresponds to the image brightness of the homogenous fully suspended system (maximum agitation rate investigated). The sigmoidal function of Eq. (6) was fitted to the data.

$$H(N) = \frac{1}{1 + e^{-a(N-N_0)}\ e^{-b(N-N_2)}} \quad (6)$$

The speed, N_H, required to achieve homogenous microcarrier suspension (H = 95 %) was then determined from the fitted curve. To assess that microcarrier concentration did not influence the calculated suspension speed, suspension of Hillex microcarriers was compared at concentrations of 1 g/L and 8 g/L. Resulting data of solution homogeneity as a function of impeller agitation rate were in close agreement, indicating that varying microcarrier concentration within this range did not influence the outcome.

2.4. *Flow characterisation*

Flow field characterisation of each of the vessels at the just-suspended speed was carried out using particle image velocimetry (PIV) measurements. A pulsed Nd:Yag laser (Nano L 50–100, Litron, UK) with a 2 × 50 mJ power output rating and wavelength of 532 nm was used. The PIV apparatus used is described in detail by Delbridge et al., (Delbridge, 2023). Measurements were taken at four vertical planes in the A-STR, denoted θ = 0°, 90°, 180°, and 270° based on their azimuthal coordinate (Fig. 1a). Given the symmetry of the S-STR vessel, and hence assumed flow field symmetry, measurements were taken in one plane. The same was assumed when capturing flow field data for the unbaffled A-STR. Ultrapure Milli-Q water was used as the working fluid and seeded with 1–20 μm rhodamine-coated polymethyl methacrylate particles to obtain 10–15 particles per interrogation grid cell. The timestep between image pairs was adjusted between 1.2 and 1.8 ms depending on the impeller agitation rate at N_{JS}, which ranged from 30 to 125 rpm. This was done to achieve a particle displacement between image pairs of ¼ of the interrogation cell grid length (Raffel, 2018), with lower impeller agitation rates requiring a larger timestep to accurately capture particle motion and vice versa. Raw images were processed using PIVlab software (Thielicke and Sonntag, 2021). A two-pass adaptive correlation analysis was used, with an initial interrogation window size of 32 × 32 pixels and a final size of 16 × 16 pixels, with a 50% interrogation area overlap. The final resolution was thus 8 × 8 pixels, corresponding to a spatial resolution of 4.8×10^{-4} m. Post-processing was used to filter images based on image contrast thresholds and velocity threshold based validation. The instantaneous velocity fields obtained were post processed using a purposely written MATLAB code to generate ensemble-averaged (mean) velocity fields. 1500 instantaneous velocity fields were used to determine the mean velocity field at each condition. This was deemed sufficient by monitoring the statistical convergence of the axial, radial, and mean velocity magnitudes at numerous points in the measured planes.

3. Results and discussion

3.1. *Power number*

Microcarrier suspension in stirred tank reactors is generally carried out at lower agitation rates than suspended animal cell culture. As a consequence, in this study, the Reynolds number often fell within the transitional regime ($10 < Re < 1 \times 10^4$). Impeller power number, N_P, in the transitional regime is not independent of Reynolds number, unlike in the turbulent regime ($Re > 1 \times 10^4$) where N_P is constant for baffled STRs. Full power curves of the baffled A-STR (UP/DP) as well as the S-STR (UP) were previously published in Delbridge et al. (Delbridge et al., 2023). Turbulent power number values of the unbaffled A-STR (UP) were also presented to demonstrate the plateau of N_P observed in the A-STR despite the absence of baffles, which is indicative of the natural baffling provided by the cubical A-STR geometry. The turbulent power number of the A-STR was determined to be

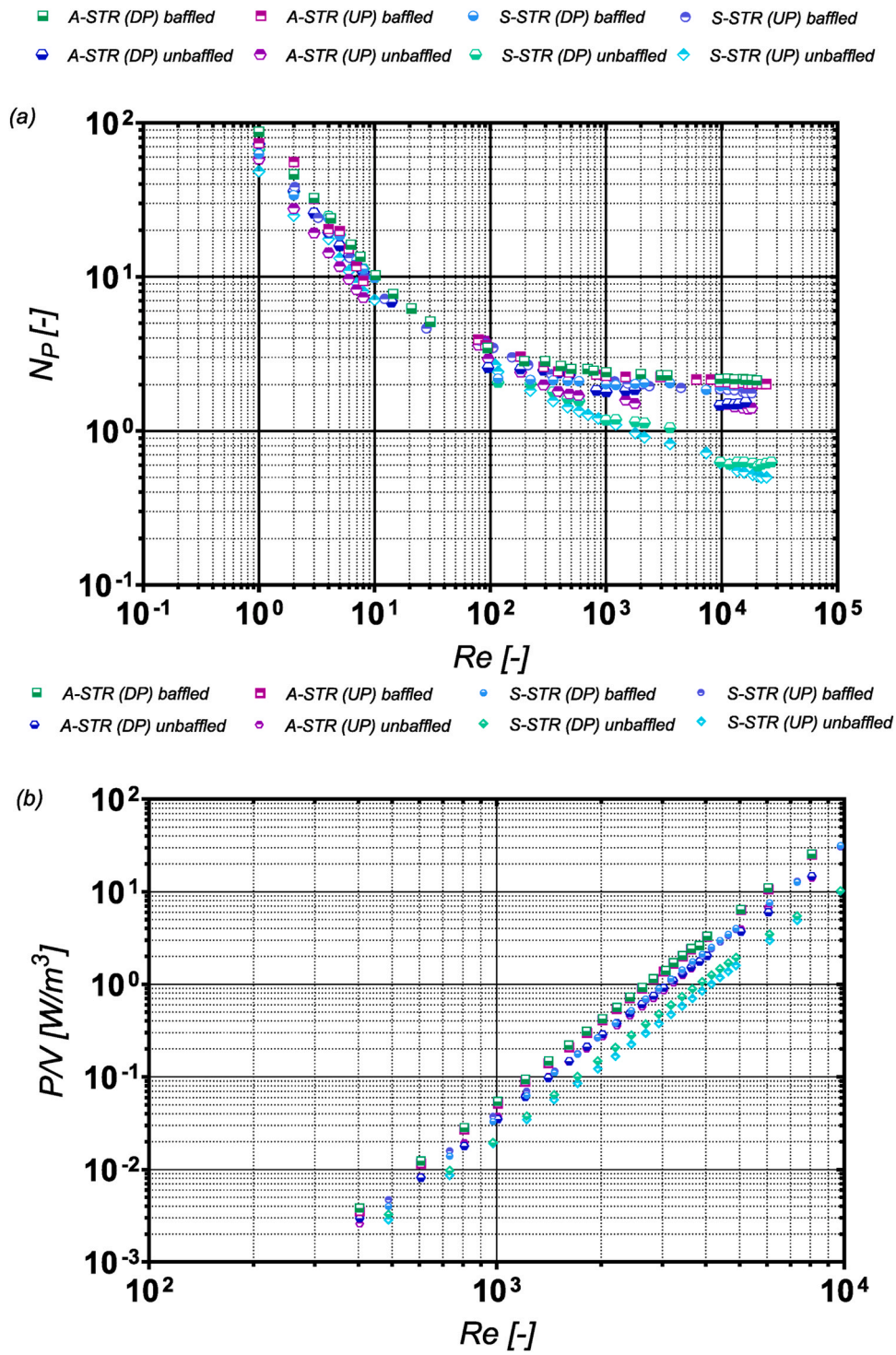

Fig. 2 – (a) Variation of impeller power number, N_P, from the laminar to turbulent regimes. For comparative purposes, curves for the baffled A-STR (UP/DP) as well as the baffled S-STR (UP) have been extracted from Delbridge et al. (2023). Error bars plotted representing standard deviation from the mean (n = 3) not visible due to high reproducibility of force readings; (b) Volumetric power input, P/V (W/m^3), as a function of Re [-]. Data for the baffled A-STR (UP ⬒ /DP ⬓) and S-STR (UP ◓/DP ◒) are compared to that of the unbaffled A-STR (UP ⬘/ DP ⬙) and unbaffled S-STR (UP ◈/DP ◈).

N_P = 2.11 and N_P = 2.17 in UP and DP mode respectively (Delbridge et al., 2023). For the S-STR operating in the turbulent regime, N_P = 1.81 (UP) and N_P = 2.09 (DP) (Delbridge et al., 2023). Given the variation of N_P throughout the agitation range for which suspension was assessed, full power curves of both vessel geometries are presented in UP/DP mode, with and without baffles (Fig. 2a). In addition, power input per unit volume (P/V) is presented across the investigated range of Re for suspension characterisation (Fig. 2b).

The power curves (Fig. 2a) of the A-STR reach a constant value in both UP and DP mode, for the baffled and unbaffled configurations. In DP mode, the average turbulent power number plateaus at N_P = 1.49 in the unbaffled A-STR, a 31.3 % decrease from the corresponding baffled power number. In UP mode a plateau is reached at N_P = 1.4 as previously shown (Delbridge et al., 2023). The unbaffled S-STR, however,

exhibits a continuous decline in N_P as Re increases. In the unbaffled S-STR (DP), N_P decreases to approximately $N_P = 0.63$ at Re $= 2.1 \times 10^4$. In the unbaffled S-STR (UP), the power number reaches as low as $N_P = 0.5$ at Re $= 2.4 \times 10^4$. Re was not increased above these magnitudes due to high fluctuations of force readings observed as a consequence of central vortex formation and bubble entrainment. The observed drop in power number is expected for unbaffled cylindrical vessels, due to solid body rotation (Kaiser et al., 2017), which is known to cause poor mixing in comparison to baffled configurations (Ciofalo et al., 1996). Suspension characterisation to follow (Section 3.2) is compared on the basis of volumetric power input (P/V), as mammalian cell culture applications are commonly scaled based on maintaining constant power input per unit volume. Volumetric power input is thus presented across the range of Re investigated, given the change in power number occurring across the transitional regime. It should be noted that the power input calculated in this work is under ungassed conditions, while cell culture applications will generally involve the introduction of a gas phase to the culture media by use of a sparger. Published work characterising power number of an Elephant Ear impeller at varied gas flow rates found that N_P was independent of the sparger flow rate when operating in up-pumping mode (Zhu et al., 2009). High air flow rates were found to cause impeller flooding in down-pumping mode, reducing N_P by up to 30 % (Zhu et al., 2009). The ring sparger of the Allegro STR range may however prevent this, given the improved distribution of gas outlets compared to the sparger used by Zhu et al. (2009). However, in light of these findings, P/V values used as a scaling parameter for the suspension studies may differ to the gassed power input per unit volume, which is used in reality to scale biological processes, and variation of P/V at high air flow rates should be considered in future studies.

3.2. *Suspension characterisation*

Suspension of four commercially available microcarriers was compared in the A-STR and S-STR in UP/DP mode. It should be noted that down-pumping mode is generally recommended for microcarrier suspension using an Elephant Ear impeller (Collignon et al., 2010; Nienow et al., 2016). However, UP mode was also assessed in this work for comparative purposes as it is commonly used for commercial bioreactors like the Allegro STR range. Hillex II microcarriers were assessed as a higher density microcarrier option. Of the microcarriers considered, Cytopore 1 was selected as a macroporous microcarrier type, while the others investigated are microporous (Koh et al., 2020). Cytodex 1 and Cytodex 3 were compared to investigate the interplay between microcarrier density and diameter, as Cytodex 1 has a slightly lower density in comparison to Cytodex 3 ($\rho = 1.03$ g/cm^3 vs. $\rho = 1.04$ g/cm^3), but the diameter of Cytodex 1 particles is larger ($D_{50} = 190$ µm vs. $D_{50} = 175$ µm). Comparison of the suspension dynamics of the selected microcarriers can be used to gain insight into the relative power input requirements when characteristics such as density, diameter, and porosity are varied. Suspension of the four microcarrier types in the A-STR and S-STR are compared (Fig. 3).

Using DP mode (Fig. 3a) in the A-STR as a reference condition, suspension of the four microcarriers investigated is compared. Cytodex 1 was suspended at the lowest power input, P/V = 0.057 W/m^3. This was expected, given the relatively low density of these microcarriers ($\rho = 1.03$ g/cm^3). Despite having the same density, Cytopore 1 required 2.8 times the volumetric power input of Cytodex 1 for homogenous suspension. The average wet diameter of Cytopore 1, $D_{50} = 230$ µm, is significantly larger than that of Cytodex 1 ($D_{50} = 190$ µm), explaining the higher power input required to achieve homogenous suspension. Although having a slightly higher density, $\rho = 1.04$ g/cm^3, Cytodex 3 microcarriers reached homogenous suspension at roughly the same power input as Cytopore 1, likely due to their smaller diameter ($D_{50} = 175$ µm). Hillex II microcarriers had the highest density of the microcarriers assessed ($\rho = 1.08$–1.15 g/cm^3) and required the highest power input (1.33 W/m^3) to fully suspend. However, this is by no means an excessive power input for microcarrier suspension – Rafiq et al. (2017) cultured hMSCs achieving high viability in the Ambr® 15 at P/V = 9.49 W/m^3. In UP mode in both reactor configurations (Fig. 3b), a similar trend is exhibited in terms of power input required to suspend each of the four microcarrier types based on their respective densities and particle diameters.

Comparing the A-STR and S-STR is useful to determine the suitability of the EE impeller for microcarrier suspsension in these vessels, given the popularity of this impeller in bioprocessing applications. As previously mentioned, the S-STR is slightly larger in diameter than the A-STR, corresponding to a 10 % volume increase at the same liquid height to tank diameter ratio as the A-STR ($H_L/T = 1.1$). In agreement with published literature (Buurman et al., 1986; Harrison et al., 2020; Jirout et al., 2020) suspension in the vessels is compared on the basis of constant power input per unit volume. In DP mode (Fig. 3a), on average for the four microcarrier types investigated, the A-STR required a 77 % power input reduction compared to the S-STR (DP) to achieve homogenous suspension. In UP mode (Fig. 3b), the A-STR and S-STR performed differently, depending on microcarrier characteristics. The specific power input required to achieve homogenous suspension was 41% lower on average in the A-STR for Cytodex 1 and Cytodex 3. On the other hand, the larger/higher density microcarriers assessed (Cytopore 1 and Hillex II) suspended at 31.9 % lower P/V in the S-STR. On average for the four microcarriers assessed, the power input required to achieve homogenous suspension in the A-STR (DP) was 67.8 % lower than the A-STR (UP) and 66.8 % lower than the S-STR (UP). The S-STR performed better in UP mode, on average requiring 25.2% lower power input to achieve 95 % homogeneity than when operated in DP mode. Past work characterising the S-STR geometry found mixing times in UP mode to be considerably lower than DP mode, with the ensemble-averaged velocity field showing poor circulation near the surface of the S-STR in DP mode (Delbridge et al., 2023). Based on these results, the cubical geometry of the Allegro STR biocontainer appears to be highly beneficial in achieving homogenous distribution of particles/substrate when compared to standard cylindrical baffled geometries equipped with the same EE impeller in DP mode. In contrast, Giacomelli et al. (2023) found that a square flat bottom vessel was the least energy efficient to suspend solids, when compared to flat and dished bottom cylindrical tanks. This is likely due to the difference in configurations between our work and that of Giacomelli et al. (2023). For instance their use of lower impeller diameters on average, increased liquid height ($H_L/T = \sim 3.3$ vs $H_L/T \sim = 1.1$) as well as different impeller designs. Using a 4-bladed pitched blade turbine as well as an HE-3 impeller, Mitchell et al. (2008) found that N_{JS} in a square tank was lower than that of an equivalent cylindrical

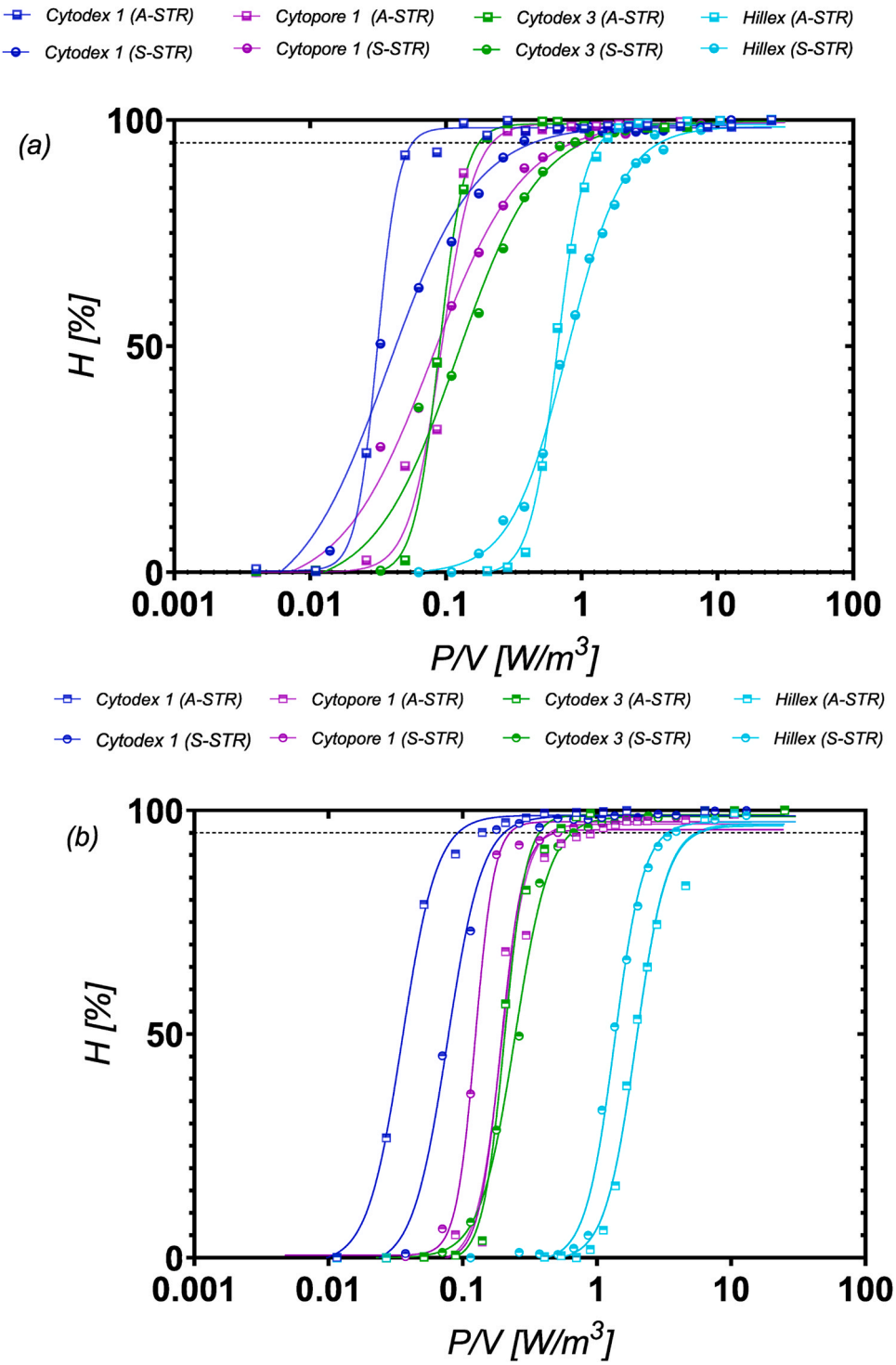

Fig. 3 – Degree of suspension homogeneity, H, with increasing volumetric power input for various commercial microcarriers in (a) the A-STR (◒) and S-STR (◒) operating in DP mode; (b) the A-STR (◓) and S-STR (◓) operating in UP mode.

tank when D/T ≥ 0.5. Our findings and those of the aforementioned studies (Mitchell et al., 2008; Giacomelli et al., 2023) suggest that square tanks exhibit improved suspension efficiency compared to cylindrical tanks at D/T ≥ 0.5 and vice versa.

The improved suspension performance of the A-STR (DP) when compared to the cylindrical S-STR is likely due to the unconventional baffling in the A-STR, which may benefit suspension performance when compared to standard baffling. Mitchell et al. (2008) deduced that baffling may be detrimental to the performance of the pitched-blade impeller by reducing tangential flow, thus requiring higher clearances for solids to suspend. The new Ambr 250 intended for microcarrier suspension applications was designed with an EE impeller and without baffles. Studies regarding microcarrier suspension in the baffled/unbaffled Ambr 250 configurations have found improved cell viabilities in the unbaffled vessels (Costariol et al., 2019; Rotondi et al., 2021). Full baffling has been suggested to reduce suspension performance, although the removal of the lower portion of baffles can improve suspension performance by allowing for tangential motion (Myers et al., 2002). The impact of baffles on suspension efficiency in the A-STR and S-STR was investigated using one microcarrier type (Fig. 4). Hillex II microcarriers were selected

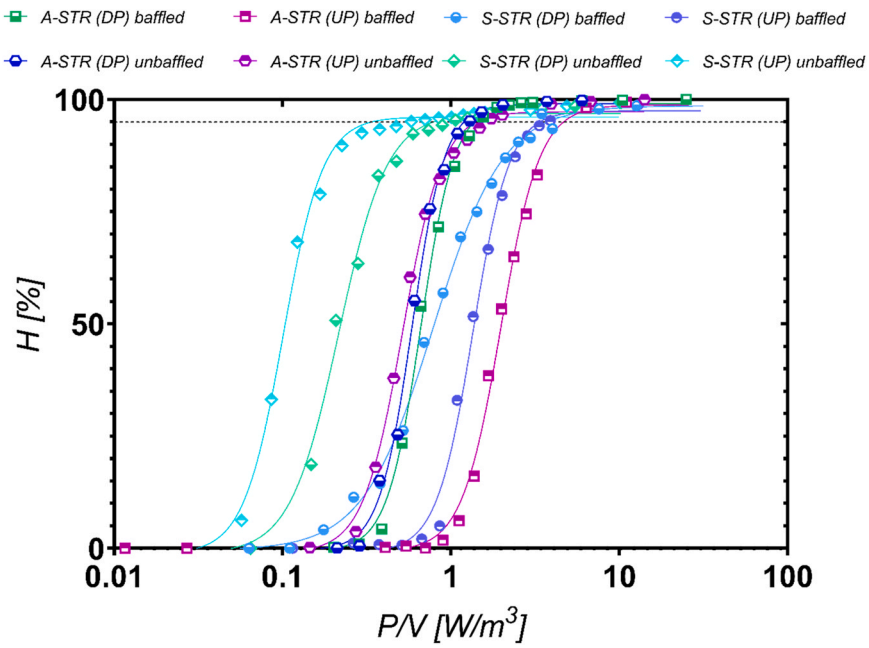

Fig. 4 – Degree of suspension homogeneity, H, of Hillex II microcarriers as a function of power input per unit volume. Data for the baffled A-STR (UP ⬒ /DP ⬓) and S-STR (UP ◓/DP ◒) are compared to that of the unbaffled A-STR (UP ⬘/DP ⬙) and unbaffled S-STR (UP ◇/DP ◈).

out of the microcarriers investigated as changes in suspension efficiency due to the removal of baffles were expected to be more pronounced for these higher density microcarriers.

The trends shown for the baffled configurations in Fig. 4 also highlight the relative power input demand in each of the configurations by direct comparison of UP with DP mode. It is clear that the baffled A-STR (DP) achieves homogenous suspension at considerably lower specific power input than the baffled A-STR (UP) and S-STR (UP/DP). In terms of the influence of baffles, both vessel configurations achieved homogenous suspension at lower power inputs when baffles were not implemented. The unbaffled A-STR achieved homogenous suspension at 66.6 % lower power input than the baffled A-STR in UP mode. The removal of baffles had a less prominent effect on the A-STR in DP mode, reducing power input demand by only 9.7 % compared to the baffled configuration. The S-STR exhibited significant reductions in power input requirements to achieve homogenous suspension in both pumping directions – P/V was reduced by 74.6 % in UP mode and by 82.9 % in DP mode in comparison to the baffled S-STR. In both tanks, baffles appear to hinder suspension performance, increasing the required power input to achieve homogenous suspension. This effect is more pronounced in the S-STR, suggesting that the more streamlined and raised baffles of the A-STR are beneficial for suspension compared to standard flat-plate baffles, particularly in DP mode where suspension performance is relatively unchanged with/without baffles. Published work showing reduced viability of CAR-T cells cultured on Dynabeads in a baffled Ambr 250 suspected that poor suspension was partly to blame, resulting in insufficient microcarrier interaction with the T-cells and consequently low proliferation when compared to the unbaffled configuration (Costariol et al., 2020). The improvement in suspension efficiency in the unbaffled cylindrical vessel in the current work further confirms this. It should be noted that the unbaffled Ambr 250 contains pH and DO probes, which at bench-scale take up a considerable amount of the vessel volume. These probes act as a form of baffles (Charalambidou et al., 2022), although their shape differs to the standard flat-plate baffles found in stirred tanks and may not reduce suspension efficiency as significantly. While the S-STR in this work achieves suspension at considerably lower power inputs without baffles present, the implications on mixing may be unfavourable as baffles are known to reduce solid body rotation and improve blend times (Myers et al., 2002). In bench scale vessels, operation without baffles may improve suspension efficiency, while the presence of relatively large internals such as probes can still result in adequate blend times. However, with scale-up the probes typically used will have negligible influence on flow structure, and the use of baffles is generally recommended. The unconventional baffles of the Allegro STR appear to allow for microcarrier suspension at reduced power input compared to standard configurations, while improving blend times. The number of impeller revolutions required to achieve 95 % homogenous suspension, Nt_H, are shown in Fig. 5.

The time to homogeneity in each vessel configuration was assessed with 8 g/l Hillex II microcarriers. Data assessed with 1 g/l Hillex II microcarriers showed reduced time to homogeneity. It is important to note that time to homogeneity can vary with microcarrier concentration, however, in this case for the purpose of comparing vessel configurations the microcarrier concentration is kept constant at 8 g/L in each configuration. Of the configurations investigated, the A-STR (DP) achieves homogenous suspension at the lowest number of impeller revolutions. The down-pumping unbaffled A-STR requires $Nt_H = 8.4$ impeller revolutions, while the baffled configuration requires $Nt_H = 8.62$ revolutions. In Fig. 4 the unbaffled S-STR (UP) was shown to achieve homogenous suspension at the lowest power input. However, Fig. 5 shows an unexpected increase in Nt_H at $P/V > 3\ W/m^3$ for this configuration. This might be explained by considering that at this speed, N = 150 RPM, a large free surface central vortex was observed in the unbaffled S-STR. The presence of such vortices is generally associated with poor axial mixing, which

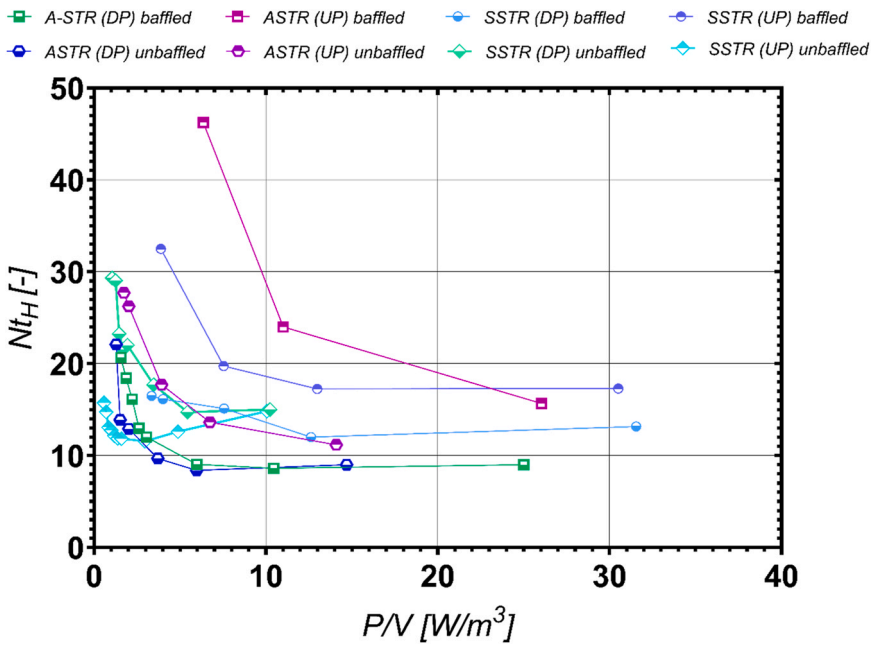

Fig. 5 – Number of impeller revolutions, Nt_H, to reach 95% suspension homogeneity in the baffled/unbaffled A-STR and S-STR in UP & DP mode. Data for the baffled A-STR (UP ⬒/DP ⬓) and S-STR (UP ◓/DP ◒) are compared to that of the unbaffled A-STR (UP ⬘/DP ⬙) and unbaffled S-STR (UP ◆/DP ◆).

could explain the increase in impeller revolutions required to reach the homogenous state. Interestingly, the unbaffled S-STR did not exhibit the same increase in impeller revolutions to homogeneity when operating in down-pumping mode. This may be due to an interaction of the upward directed impeller discharge with the central vortex formed as a consequence of no baffling, which is not as prominent in DP mode. Unlike the unbaffled S-STR (UP), the other configurations investigated generally exhibit a plateau in Nt_H. The baffled A-STR (UP) achieved homogeneity at higher power input than the other configurations investigated, and is expected to plateau at higher P/V values. The number of impeller revolutions required to achieve homogenous suspension was also shown to be constant above a critical agitation rate by Samaras, Ducci and Micheletti (Samaras et al., 2020) when investigating microcarrier suspension in a DASGIP bioreactor. To investigate the implications of the A-STR and S-STR geometries on suspension performance, a flow field analysis of the unbaffled and baffled configurations is reported in Section 3.3 to follow.

3.3. *Flow dynamics*

The PIV system described in Section 2.4 was used to assess the single-phase flow occurring in the A-STR and S-STR. Ensemble-averaged velocity magnitudes and vector maps were produced for the baffled and unbaffled A-STR and S-STR (DP mode) at the corresponding volumetric power inputs required to achieve homogenous suspension for Hillex II microcarriers (P/V = 1.33 W/m^3 and P/V = 3.35 W/m^3 respectively). These are shown in Fig. 6 (**a, b**) for the A-STR at four cross-sections, denoted as $\theta = 270°, 180°, 90°, 0°$ given that the impeller rotates clockwise in down-pumping mode. The cross-section at $\theta = 270°$ corresponds to the unbaffled face of the A-STR. Fig. 6**c** shows the flow structure of the S-STR operating at the just-suspended speed in DP mode. Velocity magnitudes are normalised with respect to impeller tip speed, V_{tip}. Despite operating at considerably lower Re, the normalised ensemble-averaged velocity fields presented in Fig. 6 are very similar to those presented in Delbridge et al. (2023) for fully turbulent flow regimes (Re > 10 000).

The overall flow field of the A-STR is characterised by a significant asymmetry across the four cross-sections investigated due to the distribution of the baffles. At $\theta = 270°$, in the unbaffled cross-section, the circulation loop is characterised by higher momentum, which is conserved along the tank wall, ~ 0.35 V_{Tip}, up to a distance of $z/H_L = 0.4$. This is not the case for the other cross-sections of the A-STR, where a smaller circulation loop is present in the lower half of the tank. These flow structures are similar to those reported in the turbulent regime by Delbridge et al. (2023)). In the current work, the maximum normalised velocity magnitudes, ~ 0.45 V_{Tip}, are slightly lower than those found in the turbulent regime, ~ 0.55 V_{Tip}. Similar observations can be made for the standard vessel geometry (Fig. 6c) where the general flow pattern and intensity scale with impeller speed despite the variation in flow regime. Given their influence on suspension efficiency, the influence of baffles on flow structure in the A-STR and S-STR was assessed. The flow structures for the unbaffled configurations of the A-STR and S-STR at N_{JS}, in DP mode, are presented in Fig. 7a, b, respectively. In this case a single cross-section of the Allegro reactor was considered sufficient to capture the general flow.

The unbaffled A-STR exhibits a very similar flow field to the unbaffled face at $\theta = 270°$ in the baffled A-STR (Fig. 6b). This is consistent with the data shown in Fig. 4 where the suspension performances were relatively similar across the baffled and unbaffled A-STR (DP). The high baffle clearance and wedge shape likely allows for more tangential motion in the impeller discharge region (Myers, Reeder and Fasano, 2002), resulting in greater lift of the settled microcarriers. In contrast, the flow field of the S-STR (DP) was altered more prominently with the removal of baffles. Most notably, in the baffled S-STR the upper region of the vessel ($z/H_L > 0.7$) is characterised by negligible velocities below 0.05 V_{tip} (Fig. 6c), while the unbaffled S-STR (Fig. 7b) exhibits velocities up to

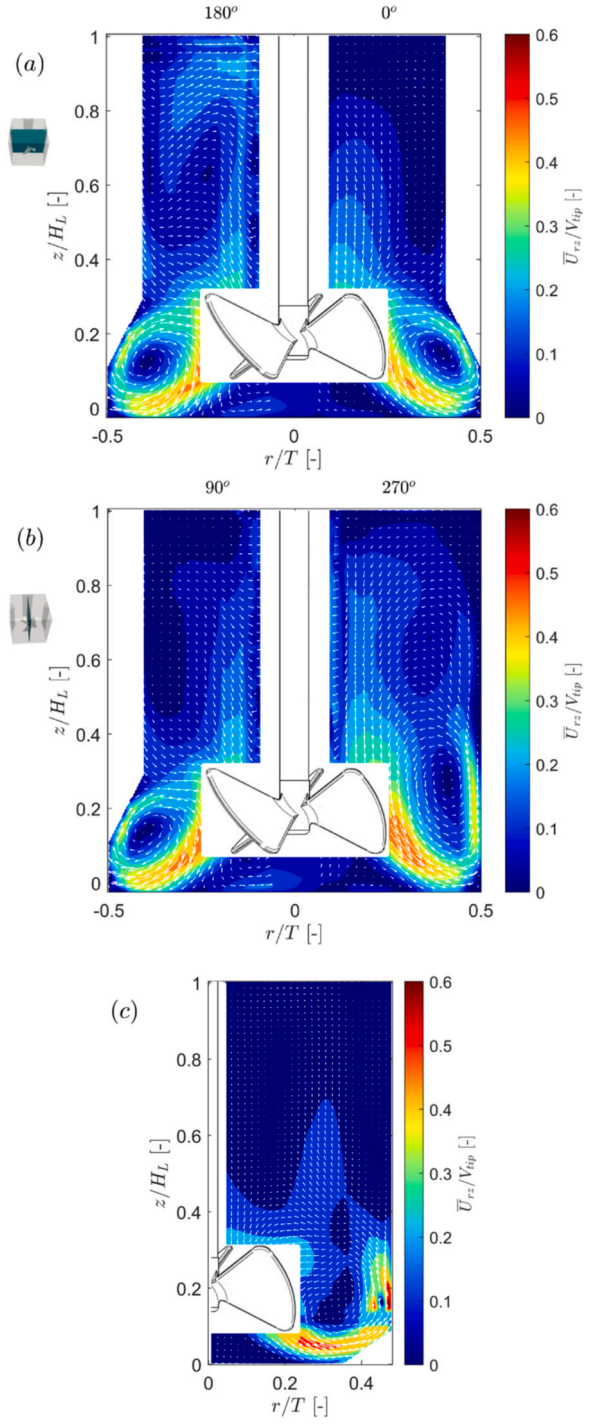

Fig. 6 – Normalised ensemble-averaged velocity magnitudes and vector map of the down-pumping EE impeller in (a) the A-STR (θ = 0°; 180°); (b) A-STR (θ = 90°; 270°); (c) S-STR. Data acquired at the just-suspended speed of Hillex II microcarriers in the A-STR (N_{JS} = 76 RPM, P/V = 1.33 W/m^3,Re = 3.1 ×10^3) and the S-STR (N_{JS} = 94 RPM, P/V = 3.35 W/m^3,Re = 4.6 ×10^3).

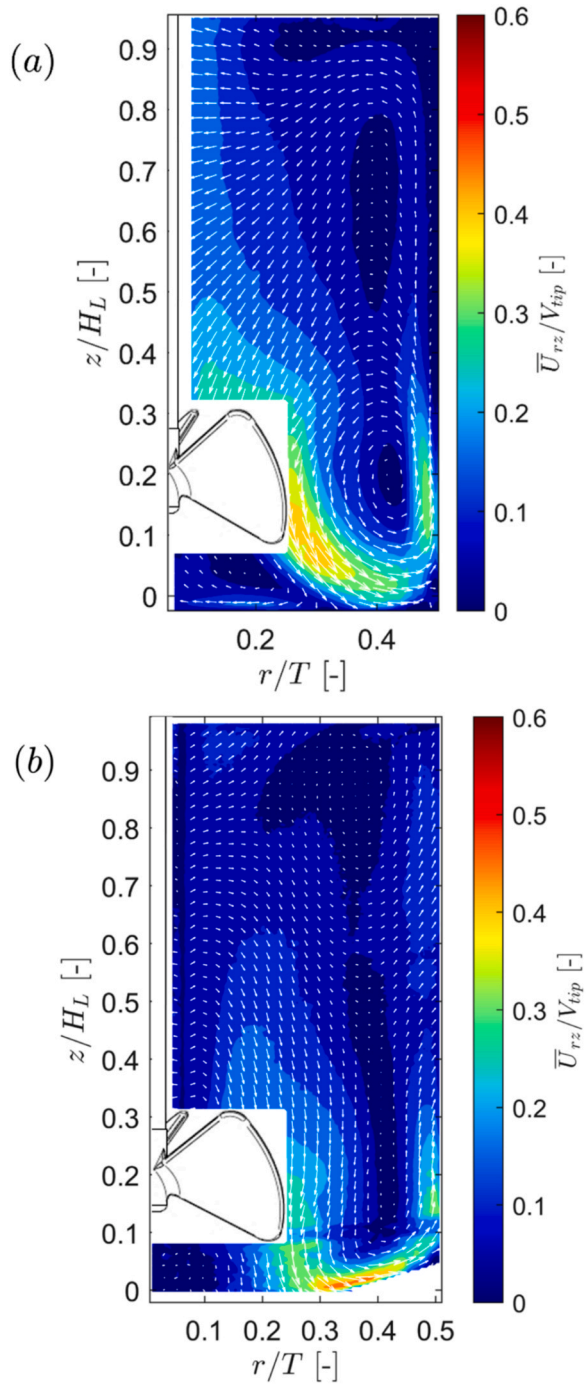

Fig. 7 – Normalised ensemble-averaged velocity magnitudes and vector map of the down-pumping EE impeller in the unbaffled (a) A-STR (N_{JS} = 83 RPM, P/V = 1.2 W/m^3,Re = 3.63 × 10^3); (b) S-STR (N_{JS} = 77 RPM, P/V = 0.96 W/m^3,Re = 3.76 × 10^3).

0.19 V_{tip} in the upper tank region. Solid body rotation as a result of the removal of baffles is likely to contribute to the lift of microcarriers at lower power inputs, however, this can hinder mixing efficiency resulting in slow mixing regions in proximity to the impeller shaft (Samaras et al., 2020; Wyrobnik et al., 2022).

In up-pumping mode, flow structures in the A-STR (Fig. 8a, b) and S-STR (Fig. 8c) at the just-suspended condition (P/V < 5 W/m^3) were in agreement with those presented by Delbridge et al. (2023) at higher power input (45 W/m^3). It should be noted that in up-pumping mode the impeller rotates anticlockwise and the cross-sections are passed in the following order, θ = 0°, 90°, 180°, 270°. The baffled A-STR required slighly higher power inputs to suspend larger and higher density microcarriers in UP mode when compared to the baffled S-STR. This is likely due to the higher velocity magnitudes below the S-STR impeller and in the upper circulation loop at the tank wall, which is not as pronounced in the A-STR (see Fig. 8). The S-STR (UP) exhibits velocity magnitudes up to 0.26 V_{tip} in the upper half of the tank, with a

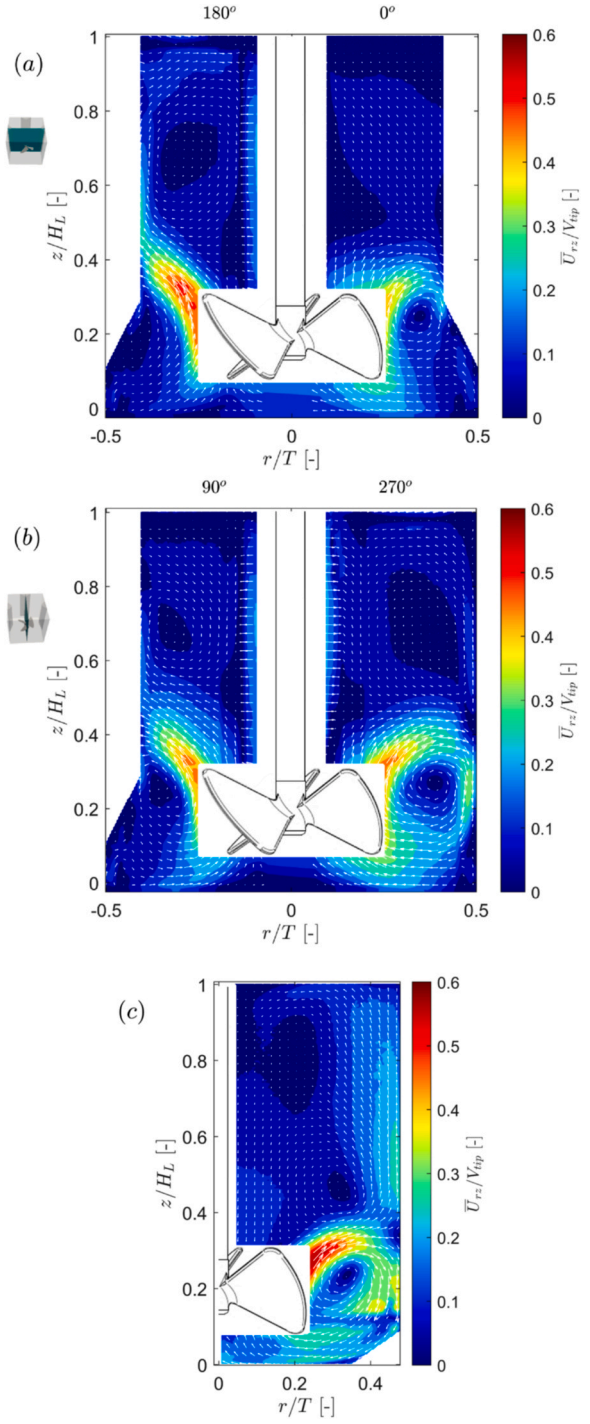

Fig. 8 – Normalised ensemble-averaged velocity magnitudes and vector map of the up-pumping EE impeller in (a) the A-STR (θ = 0°; 180°); (b) A-STR (θ = 90°; 270°); (c) S-STR. Data acquired at the just-suspended speed of Hillex II microcarriers in the A-STR (N_{JS} = 112 RPM, P/V = 4.57 W/m^3,Re = 4.52 ×10^3) and the S-STR (N_{JS} = 97 RPM, P/V = 3.7 W/m^3,Re = 4.7 ×10^3).

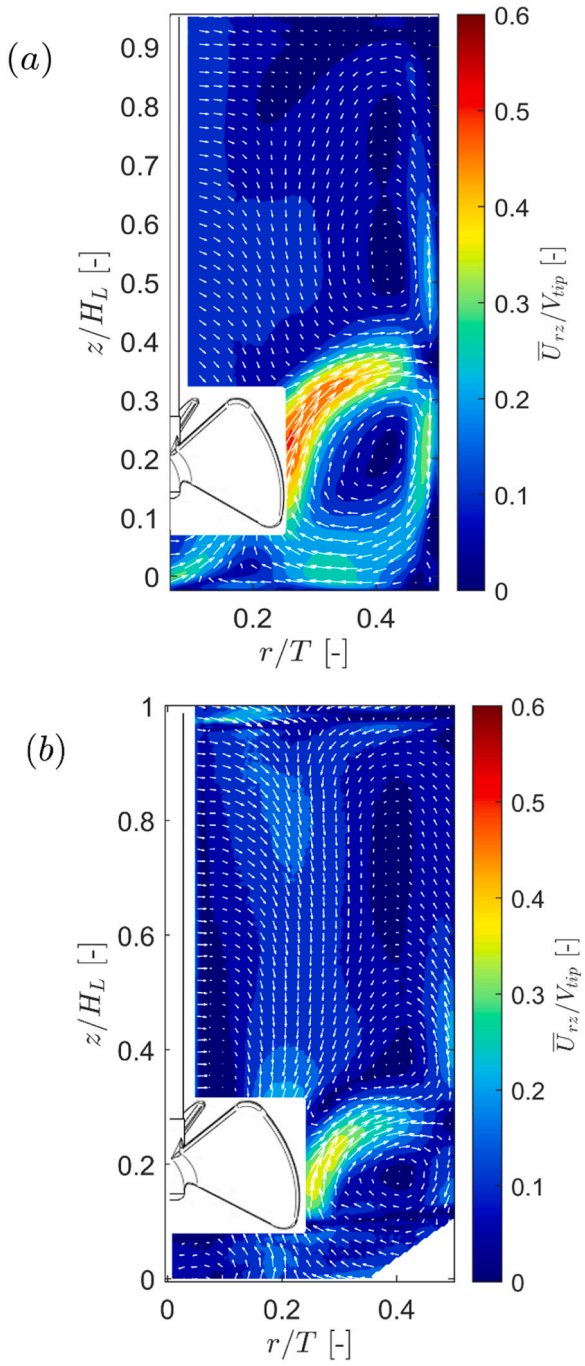

Fig. 9 – Normalised ensemble-averaged velocity magnitudes and vector map for the UP EE impeller at N_{js} of Solohill Hillex microcarriers in the unbaffled (a) A-STR (N_{JS} = 92 RPM, P/V = 2.08 W/m^3,Re = 3.7 ×10^3); (b) S-STR (N_{JS} = 70 RPM, P/V = 0.57 W/m^3,Re = 3.4 × 10^3).

visible upper circulation loop. The A-STR (UP) exhibits lower velocity magnitudes, (~0.16 V_{tip}) in the upper half of the tank when compared to the S-STR. However, the impeller discharge stream is directed upward in the cross-sections at θ = 90° and θ = 180°, due to the impeller stream being redirected as the impeller rotated anti-clockwise through the baffled planes. This is consistent with the results of Delbridge et al. (2023) for the turbulent regime, although in turbulent conditions the A-STR exhibited higher normalised velocities extending further towards the tank surface. In the A-STR (UP) at agitation rates below N_{JS}, microcarriers were observed to clear from the tank corners and subsequently pile up below the impeller. The ensemble-averaged flow field indicates low velocities in this region, hence the build up of solids. It should be noted that the commercial Allegro STR range contains a bottom mounted impeller, with a seal housing at the base, unlike the top mounted impeller used in this characterisation study. The presence of the seal housing of the commercial Allegro STR would effectively prevent solids from building up below the impeller in UP mode, likely reducing the power input required for suspension.

The removal of baffles from the up-pumping A-STR resulted in homogenous suspension at 54.8% lower power input than the UP baffled configuration. The velocity field and magnitude contour map for the unbaffled A-STR and S-STR configurations operating in UP mode are shown in Fig. 9a and b, respectively. Fig. 9a indicates higher velocity magnitudes of up to 0.28 V_{tip} below the impeller ($z/H_L < 0.1$, $r/T < 0.2$) when compared to the UP baffled A-STR where velocities only reach 0.15 V_{tip} (cf Fig. 8a, b). When comparing Fig. 9a and Fig. 8a and b it is evident that a second circulation loop is formed in the upper half of the unbaffled tank, which is not present for the baffled configuration. This could explain the reduced suspension speed and power input demand in the unbaffled configuration. This is in contrast with the lower circulation loop in proximity of the impeller which preserve an equal magnitude across the two configurations. Interestingly, in the unbaffled S-STR (UP) (Fig. 9b), the impeller discharge stream shows lower velocity magnitudes in the impeller discharge stream and lower circulation loop, but higher velocities in the secondary upper circulation loop.

4. Conclusions

The impact of baffles, bioreactor cross-section geometry and direction of impeller rotation on the power input, quality of suspension, and flow was investigated in this work. Power curves were obtained for the A-STR and S-STR in the transitional regime and a higher N_P was obtained for the A-STR. Previous work investigated turbulent power numbers of the UP/DP A-STR and S-STR, as well as that of the unbaffled A-STR in UP pumping mode. Full power curves of the A-STR (UP/DP) without baffles further confirmed the natural baffling provided by the square tank, given that in this configuration the power number reached a constant value in the turbulent regime. In contrast, the S-STR exhibited a continuous decrease in N_P as Re was increased, due to the formation of a central vortex as a consequence of solid body rotation in the absence of baffles. Suspension of four commercial microcarrier types was assessed. Generally, Cytodex 1 microcarriers were suspended at the lowest power input due to their low density ($\rho = 1.04\ g/cm^3$) while Solohill Hillex II microcarriers ($\rho = 1.11\ g/cm^3$) required considerably higher power input. The A-STR achieved homogenous microcarrier suspension at the lowest power input in DP mode. On average, for the four microcarrier types assessed, the A-STR required 67.8 % lower volumetric power input to achieve homogenous suspension in DP mode in comparison to UP mode. The A-STR outperformed the S-STR substantially in DP mode, with the S-STR requiring 77 % higher power input to achieve homogenous suspension. In general, baffles appear to negatively impact suspension efficiency. However, while probes may provide sufficient baffling for adequate blend times in bench-scale STRs, baffles are recommended to avoid solid body rotation in large-scale vessels. The wedge-shaped baffles of the Allegro STR and high baffle clearance appear to be advantageous over standard flat-plate baffles by having relatively low impact on microcarrier suspension in down-pumping mode. The A-STR with/without baffles in DP mode required the lowest number of impeller revolutions to achieve homogeneous microcarrier suspension. This is beneficial when considering intermittent agitation scenarios for microcarrier suspensions, but is also indicative of efficient circulation throughout the tank volume. Analysis of ensemble-averaged velocity magnitudes at the just-suspended speed showed that flow structures of the A-STR were mostly conserved when compared to those presented of turbulent flow conditions by Delbridge et al. (2023), despite operating at largely reduced power input and Reynolds number. This illustrates that, regardless of scale, normalised velocity fields at the just-suspended speed in the Allegro STR will be in line with those presented in this work. Flow field analysis of the unbaffled configurations generally showed higher velocity magnitudes in the upper tank regions. Considering suspension performance and mixing implications, the A-STR (DP) is recommended for achieving homogenous suspension at low power input. This is in agreement with previous work indicating homogenous distribution of kinetic energy in the A-STR (DP) when compared to other configurations, and thus implying reduced exposure of sensitive adherent cells to high shear regions.

Declaration of Competing Interest

The authors declare that they have no known competing financial interests or personal relationships that could have appeared to influence the work reported in this paper.

Acknowledgements

The authors would like to acknowledge the funding and support of the University College London – Pall Corporation Centre of Excellence and the UKRI Engineering and Physical Sciences Research Council (EPSRC) CDT Bioprocess Engineering Leadership Grant EP/S021868/1. We give special thanks to Professor Alvin Nienow, for his invaluable contribution to research in the field of mixing and biochemical engineering. Over the years, Professor Nienow became part of the Pall team, as a form of support addressing technical matters, as well as collaborating on conferences and publications regarding the Allegro STR.

References

Allan, S.J., De Bank, P.A., Ellis, M.J., 2019. Bioprocess design considerations for cultured meat production with a focus on the expansion bioreactor. Front. Sustain. Food Syst. 3 (June). https://doi.org/10.3389/fsufs.2019.00044

Bayne, K., et al., 2019. A novel, single-use bioreactor system for expansion of human mesenchymal stem/stromal cells. Cytotherapy 21 (5), S79. https://doi.org/10.1016/j.jcyt.2019.03.486

Buurman, C., Resoort, G., Plaschkes, A., 1986. Scaling-up rules for solids suspension in stirred vessels. Chemical Engineering Science 41 (11), 2865–2871. https://doi.org/10.1016/0009-2509(86)80017-3

Ciofalo, M., et al., 1996. Turbulent flow in closed and free-surface unbaffled tanks stirred by radial impellers. Chem. Eng. Sci. 51 (14), 3557–3573. https://doi.org/10.1016/0009-2509(96)00004-8

Collignon, M.L., et al., 2010. Axial impeller selection for anchorage dependent animal cell culture in stirred bioreactors: methodology based on the impeller comparison at just-suspended speed of rotation. Chem. Eng. Sci. 65 (22), 5929–5941. https://doi.org/10.1016/j.ces.2010.08.027

Collignon, M.L., et al., 2015. Hydrodynamics in a disposable rectangular parallelepiped stirred bioreactor with elliptic pendulum motion paddle. Biochem. Eng. J. 93, 212–221. https://doi.org/10.1016/j.bej.2014.10.011

Collignon, M.L., et al., 2016. Large-Eddy simulations of microcarrier exposure to potentially damaging eddies inside mini-bioreactors. Biochem. Eng. J. 108, 30–43. https://doi.org/10.1016/j.bej.2015.10.020

Costariol, E., et al., 2019. Establishing the scalable manufacture of primary human T-cells in an automated stirred-tank bioreactor. Biotechnology and Bioengineering 116 (10), 2488–2502. https://doi.org/10.1002/bit.27088

Costariol, E., et al., 2020. Demonstrating the manufacture of human CAR-T cells in an automated stirred-tank bioreactor. Biotechnol. J. 15 (9). https://doi.org/10.1002/biot.202000177

Delbridge, J.N., et al., 2023. Power, mixing and flow dynamics of the novel Allegro™ stirred tank reactor. Chem. Eng. Sci. 271, 118545. https://doi.org/10.1016/j.ces.2023.118545

Ducci, A., Yianneskis, M., 2005. Direct determination of energy dissipation in stirred vessels with two-point LDA. AIChE J. 51 (8), 2133–2149. https://doi.org/10.1002/aic.10468

Garrison, G.L., Biermacher, J.T., Brorsen, B.W., 2022. 'How much will large-scale production of cell-cultured meat cost. J. Agric. Food Res. 10 (July), 100358. https://doi.org/10.1016/j.jafr.2022.100358

Giacomelli, J.J., Grenville, R.K., Van den Akker, H.E.A., 2023. Bridging the gap between solids suspension theory and equipment design. Chemical Engineering Research and Design 190. Elsevier,, pp. 793–813. https://doi.org/10.1016/j.cherd.2022.12.015

Godoy-Silva, R., et al., 2009. Physiological responses of CHO cells to repetitive hydrodynamic stress. Biotechnol. Bioeng. 103 (6), 1103–1117. https://doi.org/10.1002/bit.22339

Godoy-Silva, R., Mollet, M., Chalmers, J.J., 2009. Evaluation of the effect of chronic hydrodynamical stresses on cultures of suspensed CHO-6E6 cells. Biotechnol. Bioeng. 102 (4), 1119–1130. https://doi.org/10.1002/bit.22146

Hanga, M.P., et al., 2020. Bioprocess development for scalable production of cultivated meat. Biotechnol. Bioeng. 117 (10), 3029–3039. https://doi.org/10.1002/bit.27469

Harrison, S.T.L., et al., 2020. Mixing indices allow scale-up of stirred tank slurry reactor conditions for equivalent homogeneity. Chemical Engineering Research and Design. Institution of Chemical Engineers 153, 865–874. https://doi.org/10.1016/j.cherd.2019.10.049

Huchet, F., Liné, A., Morchain, J., 2009. Evaluation of local kinetic energy dissipation rate in the impeller stream of a Rushton turbine by time-resolved PIV. Chem. Eng. Res. Des. 87 (4), 369–376. https://doi.org/10.1016/j.cherd.2008.11.012

Jirout, T., Rieger, F., Ceres, D., 2020. Scale-up of mixing equipment for suspensions. Processes 8 (8). https://doi.org/10.3390/PR8080909

Jossen, V., et al., 2018. Manufacturing human mesenchymal stem cells at clinical scale: process and regulatory challenges. Appl. Microbiol. Biotechnol. 102 (9), 3981–3994. https://doi.org/10.1007/s00253-018-8912-x

Kaiser, S.C., et al., 2017. Development of a method for reliable power input measurements in conventional and single-use stirred bioreactors at laboratory scale. Eng. Life Sci. 17 (5), 500–511. https://doi.org/10.1002/elsc.201600096

Koh, B., et al., 2020. Three dimensional microcarrier system in mesenchymal stem cell culture: a systematic review. Cell Biosci. 1–16. https://doi.org/10.1186/s13578-020-00438-8

Lawson, T., et al., 2017. Process development for expansion of human mesenchymal stromal cells in a 50 L single-use stirred tank bioreactor. Biochem. Eng. J. 120, 49–62. https://doi.org/10.1016/j.bej.2016.11.020

Ma, N. , Koelling, K.W. and Chalmers, J.J. , 2002. Fabrication and use of a transient contractional flow device to quantify the sensitivity of mammalian and insect cells to hydrodynamic forces. doi: 10.1002/bit.10387.

Micheletti, M., et al., 2004. On spatial and temporal variations and estimates of energy dissipation in stirred reactors. Chem. Eng. Res. Des. 82 (9 Spec. Iss.), 1188–1198. https://doi.org/10.1205/cerd.82.9.1188.44172

Mitchell, E.T., et al., 2008. Solids suspension agitation in square tanks. Can. J. Chem. Eng. 86 (1), 110–116. https://doi.org/10.1002/cjce.20004

Mollet, M. et al., 2007. Acute hydrodynamic forces and apoptosis: a complex question. doi: 10.1002/bit.21476.

Neunstoecklin, B., et al., 2015. Determination of the maximum operating range of hydrodynamic stress in mammalian cell culture. J. Biotechnol. https://doi.org/10.1016/j.jbiotec.2014.12.003

Neunstoecklin, B., et al., 2016. Pilot-scale verification of maximum tolerable hydrodynamic stress for mammalian cell culture. Appl. Microbiol. Biotechnol. 100 (8), 3489–3498. https://doi.org/10.1007/s00253-015-7193-x

Nienow, A.W., et al., 2013. Scale-down studies for assessing the impact of different stress parameters on growth and product quality during animal cell culture. Chem. Eng. Res. Des. 91 (11), 2265–2274. https://doi.org/10.1016/j.cherd.2013.04.002

Nienow, A.W., et al., 2014. A potentially scalable method for the harvesting of hMSCs from microcarriers. Biochem. Eng. J. 85, 79–88. https://doi.org/10.1016/j.bej.2014.02.005

Nienow, A.W., et al., 2016. Agitation conditions for the culture and detachment of hMSCs from microcarriers in multiple bioreactor platforms. Biochem. Eng. J. 108, 24–29. https://doi.org/10.1016/j.bej.2015.08.003

Nienow, A.W., 2021. The impact of fluid dynamic stress in stirred bioreactors – the scale of the biological entity: a personal view. Chem. -Ing. -Tech. 93 (1–2), 17–30. https://doi.org/10.1002/cite.202000176

Nienow, A.W., Isailovic, B., Barrett, T.A., 2016. Design and performance of single-use, stirred-tank bioreactors. BioProcess Int. 14 (10), 12–21 Available at: https://bioprocessintl.com/2016/design-performance-single-use-stirred-tank-bioreactors/.

Olmos, E., et al., 2015. Critical agitation for microcarrier suspension in orbital shaken bioreactors: experimental study and dimensional analysis. Chem. Eng. Sci. 122, 545–554. https://doi.org/10.1016/j.ces.2014.08.063

Pall, L.S. (2015) 'Screening studies using six-well plates and snap-top tubes', protocol, USD2991(1), pp. 1–8. Available at: www.pall.com/biopharm.

Raffel, M. et al., 2018. Particle image velocimetry: a practical guide, particle image velocimetry: a practical guide, pp. 1–32. Available at: https://doi.org/10.1007/978–3-319–68852-7_1.

Rafiq, Q.A., et al., 2013. Culture of human mesenchymal stem cells on microcarriers in a 5 l stirred-tank bioreactor. Biotechnol. Lett. 35 (8), 1233–1245. https://doi.org/10.1007/s10529-013-1211-9

Rafiq, Q.A., et al., 2017. Process development of human multipotent stromal cell microcarrier culture using an automated high-throughput microbioreactor. Biotechnol. Bioeng. 114 (10), 2253–2266. https://doi.org/10.1002/bit.26359

Samaras, J.J., Micheletti, M., Ducci, A., 2019. Suspension and mixing characterization of intermittent agitation modes in DASGIP bioreactors. Chem. Eng. Technol. 42 (8), 1587–1593. https://doi.org/10.1002/ceat.201900069

Samaras, J.J., Micheletti, M., Ducci, A., 2020. Flow, suspension, and mixing dynamics in DASGIP bioreactors: part 1. AIChE J. 1–14. https://doi.org/10.1002/aic.17014

Rotondi, M., et al., 2021. Design and development of a new ambr250® bioreactor vessel for improved cell and gene therapy applications. Biotechnology Letters. Springer Netherlands 43 (5), 1103–1116. https://doi.org/10.1007/s10529-021-03076-3

Samaras, J.J., Ducci, A., Micheletti, M., 2020. Flow, suspension and mixing dynamics in DASGIP bioreactors, Part 2. AIChE J. 66 (11), 1–15. https://doi.org/10.1002/aic.16999

Schirmaier, C., et al., 2014. Scale-up of adipose tissue-derived mesenchymal stem cell production in stirred single-use bioreactors under low-serum conditions. Eng. Life Sci. 14 (3), 292–303. https://doi.org/10.1002/elsc.201300134

Silva Couto, P., et al., 2019. First decade of clinical trials and published studies with mesenchymal stromal cells from umbilical cord tissue. Regen. Med. 14 (4), 309–319. https://doi.org/10.2217/rme-2018-0171

Silva Couto, P., et al., 2020. Expansion of human mesenchymal stem/stromal cells (hMSCs) in bioreactors using microcarriers: lessons learnt and what the future holds. Biotechnol. Adv. 45, 107636. https://doi.org/10.1016/j.biotechadv.2020.107636

Thielicke, W., Sonntag, R., 2021. Particle image velocimetry for MATLAB: accuracy and enhanced algorithms in PIVlab. J. Open Res. Softw. 9, 1–14. https://doi.org/10.5334/JORS.334

Wyrobnik, T.A., et al., 2022. Engineering characterization of the novel Bach impeller for bioprocessing applications requiring low power inputs. Chem. Eng. Sci. 252, 117263. https://doi.org/10.1016/j.ces.2021.117263

Zhu, H., et al., 2009. Mixing studies in a model aerated bioreactor equipped with an up- or a down-pumping "Elephant Ear" agitator: power, hold-up and aerated flow field measurements. Chem. Eng. Res. Des. 87 (3), 307–317. https://doi.org/10.1016/j.cherd.2008.08.013

Myers, K. J., Reeder, M. F. and Fasano, J. B. (2002) 'Optimize Mixing by Baffles', *CEP Magazine,* (February issue), pp. 42–47.

Charalambidou, A. D. et al. (2022) 'The impact of baffles and probes on flow and power consumption in single- use bioreactors', *Single-Use Technologies V: Building The Future*. Available at: https://dc.engconfintl.org/sut_v/50 (Accessed: 11 May 2023).